Acta Pharmaceutica Sinica B 2024;14(1):241−255

Chinese Pharmaceutical Association
Institute of Materia Medica, Chinese Academy of Medical Sciences

Acta Pharmaceutica Sinica B

www.elsevier.com/locate/apsb
www.sciencedirect.com

ORIGINAL ARTICLE

GRK2 inhibits Flt-1$^+$ macrophage infiltration and its proangiogenic properties in rheumatoid arthritis

Xuezhi Yang[a,†], Yingjie Zhao[b,†], Qi Wei[a,†], Xuemin Zhu[a], Luping Wang[a], Wankang Zhang[a], Xiaoyi Liu[a], Jiajie Kuai[a], Fengling Wang[a], Wei Wei[a,*]

[a]*Institute of Clinical Pharmacology, Anhui Medical University, Key Laboratory of Anti-Inflammatory and Immune Medicine, Anhui Collaborative Innovation Center of Anti-Inflammatory and Immune Medicine, Ministry of Education, Hefei 230032, China*
[b]*Department of Clinical Pharmacology, the Second Affiliated Hospital of Anhui Medical University, Hefei 230601, China*

Received 5 June 2023; received in revised form 4 September 2023; accepted 15 September 2023

KEY WORDS

GRK2;
Monocyte-derived macrophages;
Rheumatoid arthritis;
PPARγ;
Flt-1

Abstract Rheumatoid arthritis (RA) is an autoimmune disease with a complex etiology. Monocyte-derived macrophages (MDMs) infiltration are associated with RA severity. We have reported the deletion of G-protein-coupled receptor kinase 2 (GRK2) reprograms macrophages toward an anti-inflammatory phenotype by recovering G-protein-coupled receptor signaling. However, as more GRK2-interacting proteins were discovered, the GRK2 interactome mechanisms in RA have been understudied. Thus, in the collagen-induced arthritis mouse model, we performed genetic *GRK2* deletion using *GRK2*$^{f/f}$*Lyz2*-Cre$^{+/-}$ mice. Synovial inflammation and M1 polarization were improved in *GRK2*$^{f/f}$*Lyz2*-Cre$^{+/-}$ mice. Supporting experiments with RNA-seq and dual-luciferase reporter assays identified peroxisome proliferator-activated receptor γ (PPARγ) as a new GRK2-interacting protein. We further confirmed that fms-related tyrosine kinase 1 (Flt-1), which promoted macrophage migration to induce angiogenesis, was inhibited by GRK2-PPARγ signaling. Mechanistically, excess GRK2 membrane recruitment in CIA MDMs reduced the activation of PPARγ ligand-binding domain and enhanced Flt-1 transcription. Furthermore, the treatment of mice with GRK2 activity inhibitor resulted in significantly diminished CIA pathology, Flt-1$^+$ macrophages induced-synovial inflammation, and angiogenesis. Altogether, we anticipate to facilitate the elucidation of previously unappreciated

*Corresponding author.
E-mail address: wwei@ahmu.edu.cn (Wei Wei).
†These authors made equal contributions to this work.
Peer review under the responsibility of Chinese Pharmaceutical Association and Institute of Materia Medica, Chinese Academy of Medical Sciences.

https://doi.org/10.1016/j.apsb.2023.09.013

details of GRK2-specific intracellular signaling. Targeting GRK2 activity is a viable strategy to inhibit MDMs infiltration, affording a distinct way to control joint inflammation and angiogenesis of RA.

1. Introduction

Rheumatoid Arthritis (RA) is a systemic autoimmune disorder, affecting approximately 1% of the population worldwide[1]. Approximately 75% of patients without timely treatment will develop joint deformities and disabilities within 3 years. Therefore, the treatment of RA urgently requires a rational therapeutic approach that can alleviate synovial inflammation and reverse bone erosion.

Increasing evidence supports the key role of synovial macrophages (SMs) in the pathogenesis of RA[2]. For example, their numbers increase during active disease; their numbers decrease after effective treatment. We[3] and others[4,5] revealed that SMs mainly consist of monocyte-derived macrophages (MDMs) and tissue-resident macrophages. In several animal models of arthritis[6–8], the specific intra-articular depletion of tissue-resident SMs led to the development of accelerated arthritis, while the depletion of both circulating monocytes and synovial MDMs markedly reduced the severity of RA. Reprogramming the inflammatory phenotypes of recruited synovial MDMs contributes to arthritis remission. Directly targeting macrophages is promising, but there are still challenges, such as how to discriminate between non-activated and activated macrophages. In addition, for the specific elimination of inflammatory macrophages in RA, no therapy has been shown to be both effective and safe. Although tumor necrosis factor-α (TNF-α) inhibitors and other inflammatory factor inhibitors are beneficial for the treatment of RA, they also disrupt normal immune regulation function and lead to serious adverse reactions[9]. Limitations in current therapies have prompted investigations for developing safe, novel pharmacological treatments to regulate synovial MDMs in RA.

G-protein-coupled receptor kinase 2 (GRK2) is part of a cluster of kinases associated with the rapid desensitization of G-protein-coupled receptors (GPCRs). We and others have shown that elevated GRK2 expression in RA and other diseases led to the loss of physiologic GPCR signaling[10–18]. Research on GRK2 has primarily focused on the desensitization of GPCR. In addition to its canonical function, GRK2 performs several other functions, including binding to and regulating a variety of cellular proteins involved in diverse signal transduction pathways *via* kinase-independent mechanisms[15]. Directly targeting GRK2 makes sense since most cytokines function *via* the GRK2 signaling pathway. It appears warranted to develop small-molecule inhibitors of GRK2 since no GRK2 inhibitors have been approved for market yet. We have recently reported the therapeutic efficacy of a new compound paeoniflorin-6′-*O*-benzene sulfonate (CP-25), which reduced GRK2 membrane recruitment by targeted inhibition of GRK2 Ala321[13]. We also found that GRK2 deletion drove M2 polarization by restoring the GPCR pathway[19]. However, the GRK2 interactome and its modulation mechanisms in RA MDMs have been understudied.

Here, using peripheral blood mononuclear cells (PBMCs) and synovial tissue from healthy control (HC), osteoarthritis (OA), and RA patients, we studied changes in MDMs and their relation to GRK2. Furthermore, we investigated the role of GRK2 inhibition (using *GRK2*$^{f/f}$*Lyz2*-Cre$^{+/-}$ mice) on MDMs of collagen-induced arthritis (CIA) mouse model. Mechanistically, we identified GRK2-interacting protein and downstream signaling by RNA-seq and dual-luciferase reporter. Our results provide a distinct way to control joint inflammation and angiogenesis of RA.

2. Materials and methods

2.1. Procurement of human PBMC and synovium

An institutional review board-approved protocol was executed to collect discarded deidentified peripheral blood and synovium from patients. Peripheral blood was obtained from 22 patients with RA and 10 healthy controls (HC). PBMC collection and processing are as described[37]. We obtained HC synovium (from patients undergoing arthroscopic surgery after traumatic fractures, $n = 3$), OA synovium (from patients undergoing arthroplasty, $n = 3$) and RA synovium (from patients undergoing arthroplasty, $n = 5$). Synovium was fixed in formalin and embedded in paraffin; 10 μm sections were used for IHC staining and IF staining.

2.2. Animal studies

Seven-week-old male DBA/1 mice, ten-week-old male C57BL/6J mice, GRK2$^{f/f}$ mice and Lyz2-CreER^{T2}mice were purchased from GemPharmatechco. CCR2$^{GFP/GFP}$ mice were purchased from The Jackson Laboratory. PPARγ *KO* mice were donated by Xiaofeng Li at Anhui Medical University. All mice were housed in groups of five mice per microisolator cage in a room with a 12 h light/dark schedule. All experiments were approved by the Ethics Review Committee for Animal Experimentation of Institute of Clinical Pharmacology, Anhui Medical University, China.

2.3. The establishment and evaluation of CIA model

2.3.1. DBA mice

Induction of CIA was induced and assessed as previously described[18]. Mice were divided into normal, CIA model, CP-25 and Ecep treatment group ($n = 8$ per group). The normal and CIA mice were given an equal volume of vehicle.

2.3.2. C57BL/6 background mice

Induction of CIA was induced and assessed as described[38]. Male mice aged 10-weeks-old were immunized with the emulsion of complete Freund's adjuvant (CFA, 4 mg/mL) and chicken type II collagen (CII, 4 mg/mL) in a 1:1 mixture (total 100 μL)

intradermally into the base of the tail on Day 0. The booster immunization of CII (4 mg/mL) with incomplete Freund's adjuvant (IFA, 4 mg/mL) was performed intrademally in a site proximal to the first injection site on Day 14. All reagents were purchased from Chondrex. Onset occurs 4 weeks after initial immunization. CKO mice were divided into GRK2$^{f/f}$, GRK2$^{f/f}$ + CIA, GRK2$^{f/f}$Lyz2-Cre$^{+/-}$ and GRK2$^{f/f}$Lyz2-Cre$^{+/-}$+CIA group (n = 5 per group).

2.3.3. Evaluation of CIA arthritis

An evaluation of the severity of the CIA was performed by two independent observers with no knowledge of the treatment protocol. The arthritis index and arthritis severity in each group was evaluated once every 3 days as follows. Arthritis index: 0 = no arthritis; 1 = swelling and/or redness of the paw or one digit; 2 = two arthritic joints; 3 = more than two joints involved; 4 = severe arthritis of the entire paw and all digits. The maximum arthritis index of each mouse was 16[18]. Arthritis severity: 0 = normal hind paw; 1 = hind paw with mild swelling; 2 = hind paw with pronounced edematous swelling; 3 = hind paw with ankylosis; The maximum arthritis severity of each mouse was 12[40]. Arthritis index and severity were evaluated using the Mann−Whitney U test. Modeling animals without swelling were excluded.

2.4. Drug treatment studies

In CIA model established by DBA mice, the normal and model group received the vehicle (5% CMC), the CP-25 treatment group received CP-25 (35 mg/kg) gavage administered daily, and the Ecep treatment group was administered Ecep (4.5 mg/kg) daily by intraperitoneal injection.

2.5. Cell culture

SMs were isolated from the synovium of RA patients and mice. SMs were plated into type IV collagenase and incubate for 2 h with shaking. After incubation, cells were collected by centrifugation (2500 rpm, 5 min).

BMDMs were isolated from the femurs of mice. BMDMs were plated into sterile Petri dishes and incubated in DMEM supplemented with 10% FBS and 10% M-CSF-conditioned media. BMDMs were incubated at 37 °C with 5% CO_2 and harvested after 7 days.

Raw264.7 and constructed GRK2$^{-/-}$ Raw were cultured as previously described[18].

PBMC were isolated from whole blood using Ficoll−Paque plus washed with PBS and maintained in RPMI-1640 (Gibico) supplemented with 10% FBS for further use.

HUVEC were cultured as described previously[39]. HUVEC were purchased from ATCC and incubated at 37 °C with 5% CO_2.

2.5.1. 3D cell culture

We cultured MDMs of PBMC origin using a PrimeSurface 96U 3D cell culture plate, and collected by careful centrifuge at 300×g for 3 min for flow cytometry analysis. We also stained 3D spheres with DAPI to observed cell morphology by high-content imaging (Molecular Devices).

2.6. Western blot

Western blot analysis was performed as previously described[18]. The dilution of primary antibody of CCR2, iNOS, Arg1, GRK2, PPARγ, Flt-1, ATPB2, GAPDH, tubulin and β-actin are 1:500−1:1000. The dilution of second primary antibody of goat anti-mouse is 1:10,000, of goat anti-rabbit is 1:10,000. The membranes were scanned with an ImageQuant LAS 4000 (GE Healthcare) and analyzed used ImageJ software.

2.7. Histological examination

The ankle joints of mice were immersed in 10% formalin, then decalcified and paraffin-embedded. Sections (3 μm each) were used for H&E, Safranin O and Toluidine blue staining.

2.7.1. H&E staining

H&E staining were performed as previously described[18].

2.7.2. Safranin O staining

The sections were immersed in Safranin O staining solution for 5 min. After washing, the slides were stained with fast green staining solution for 2 min. The slides were put into 1% acetic acid for 30 s. After washing, the slides were dehydrated with 95% ethyl alcohol and xylene. Slides were mounted using neutral gum.

2.7.3. Toluidine blue staining

The sections were dehydrated in methanol, washed in PBS and stained in 0.1% toluidine blue for 30 min.

2.8. IHC, mIHC and IF staining

IHC and IF staining were performed as previously described[13,18]. IHC was using the PV-6000 two-step immunohistochemistry kit to perform the blocking and antibody incubation. For IF, 0.5% BSA was used to block the unspecific antigens. After primary and secondary antibodies incubation, DAPI was used to co-stain. IHC and IF stained sections were imaged using Pannoramic MIDI Slide scanner (3D HISTECH).

mIHC was using the multiple fluorescent immunohistochemical kit (Panovue, TSA-RM-275). Three primary (PPD520, PPD570, PPD650) and secondary antibodies were incubated successively, finally DAPI was used to co-stain. mIHC stained sections were imaged by confocal microscopy. Image was analyzed using Indica Halo software.

2.9. ILβ-1-dependent acute inflammatory arthritis

CCR2$^{GFP/GFP}$ mice were injected intraarticularly with mBSA on Day 0 and subcutaneously with recombinant human IL-1β on Day 0 to Day 2. CCR2$^{GFP/GFP}$ mice were sacrificed at Day 7[40].

2.10. CO-IP and his pull-down

Cells were collected and washed three times with PBS and lysed in lysis buffer (purchased from beyotime, P0013) with protease inhibitors for 30 min on ice, then samples were centrifuged at 12,000×g for 15 min. The lysate was precleaned by IgG-coated protein A/G plus-agarose beads and then mixed with the indicated primary antibody coated beads and incubated overnight at 4 °C. The immune complexes were collected and eluted with 5 × 330 SDS loading buffer, and which were then subjected to immunoblotting[41,42].

His pull-down was carried out according to standard protocol from previous studies[13]. His-GRK2 plasmid was synthesized by Generalbiol Co.

2.11. FRET experiment

HEK293 cells infected with si*GRK2* or si*PPARγ* were co-transfected with mCherry-GRK2 and EGFP-PPARγ, fixed 8 h posttransfection, imaged by confocal microscopy. Specific FRETc signals were calculated. Panels show representative cells. Bars are 3 μm.

2.12. Statistical analyses

One-way or two-way analysis of variance, Student's *t*-tests and rank sum tests were used to determine the differences between experimental groups. Results are shown as means ± SEM. P value < 0.05 was regarded as a significant difference. All calculations were performed using the GraphPad Prism 8.3 program.

2.13. Ethics approval

This study involves human participants and was approved by the Ethics Committee of Anhui Medical University.

3. Results

3.1. GRK2 is closely correlated with synovial MDMs in RA

Changes in GRK2 in RA synovial macrophages have not been investigated. Reportedly, $CD14^+$ PBMCs correlated well with paired synovial fluid mononuclear cells in patients with RA, and monocyte recruitment was determined by measuring chemokine (C−C motif) receptor 2 (CCR2) expression[20−22]. Thus, we detected GRK2 expression in $CD14^+CCR2^+$ PBMCs of RA. The ratio of $CD14^+CCR2^+$ (Fig. 1a) and GRK2 expression (Fig. 1b) were significantly increased in RA PBMCs compared with HC. Additionally, high correlations were achieved between GRK2 levels and $CD14^+CCR2^+$ and RA-related clinical manifestations, including disease activity score 28 (DAS28), erythrocyte sedimentation rate (ESR), and visual analog scale (VAS) (Fig. 1c).

OA was often used as a disease control for RA in previous studies[23]. However, elevated GRK2 has also been reported in OA synovium, and was not further compared with RA[15]. We collected three HC, three OA, and five RA synovium, and the expression of GRK2 (Fig. 1d) and CD68 (Fig. 1f) increased in both OA and RA compared with HC synovium, while CCR2 (Fig. 1e) expression only increased in RA synovium. GRK2 expression increased in RA synovium compared with OA synovium, suggesting that GRK2 may be more related to synovial inflammation. Compared with M-CSF-stimulated PBMCs of HC (Fig. 1g), GRK2 membrane expression increased in RA SMs (Fig. 1h). We further treated RA SMs with the GRK2 activity inhibitor GSK180736A, and the expression of inducible nitric oxide synthase (iNOS) and CCR2 decreased, while arginase-1 (Arg1) increased (Fig. 1i). These data suggested that GRK2 was closely correlated with the activation of infiltrated MDMs in the RA synovium.

3.2. GRK2 deficiency attenuates the development of CIA

To test the GRK2-specific intracellular signaling in RA MDMs, we generated mice with myeloid-cell-specific *GRK2* deficiency (referred to as $GRK2^{f/f}Lyz2\text{-}Cre^{+/-}$) (Supporting Information Fig. S1). $GRK2^{f/f}$ and $GRK2^{f/f}Lyz2\text{-}Cre^{+/-}$ mice were subjected to CIA (Fig. 2a), a standard murine model of arthritis resembling human RA. Compared with that in the CIA $GRK2^{f/f}$ mice, the arthritis severity (Supporting Information Fig. S2a) and arthritis index (Fig. S2b) in the CIA $GRK2^{f/f}Lyz2\text{-}Cre^{+/-}$ mice were relieved. We also used H&E, toluidine blue, and safranin O fast green staining to study pathological changes in the ankle joint. Paw swelling, synovial inflammation, bone erosions, and the number of osteoclasts of $GRK2^{f/f}Lyz2\text{-}Cre^{+/-}$ mice were lower than that of $GRK2^{f/f}$ mice (Fig. S2c). Quantitative levels of 23 cytokines in murine serum were assayed through LX-MultiDTM-23 technology (Fig. S1d−S1f). We classified these 23 cytokines in terms of inflammatory cytokines, anti-inflammatory cytokines, and chemokines. Compared to CIA $GRK2^{f/f}$ mice, the expression of the inflammatory cytokines IL-1β, IL-5, IL-6, IL-9, IL-12p40, TNF-α, and interferon-γ (IFN-γ) was lower in CIA $GRK2^{f/f}Lyz2\text{-}Cre^{+/-}$mice. The expression of IL-1α, IL-3, and IL-12p70 was higher in CIA $GRK2^{f/f}Lyz2\text{-}Cre^{+/-}$ mice (Fig. S2d). Compared to CIA $GRK2^{f/f}$ mice, the expression of the chemokines CCL2, CCL11, and CXCL1 was higher in CIA $GRK2^{f/f}Lyz2\text{-}Cre^{+/-}$ mice. The expression of CCL3 and CCL4 was lower in CIA $GRK2^{f/f}Lyz2\text{-}Cre^{+/-}$ mice (Fig. S2e). Compared to CIA $GRK2^{f/f}$ mice, the expression of anti-inflammatory cytokines IL-4, IL-10, and C-SCF were higher in CIA $GRK2^{f/f}Lyz2\text{-}Cre^{+/-}$ mice. The expression of IL-13 was lower in CIA $GRK2^{f/f}Lyz2\text{-}Cre^{+/-}$ mice (Fig. S2f). In summary, a balance of most pro- and anti-inflammatory subset phenotypes was restored in CIA $GRK2^{f/f}Lyz2\text{-}Cre^{+/-}$ mice. However, most of the cell migration-related parameters were higher in CIA $GRK2^{f/f}Lyz2\text{-}Cre^{+/-}$ mice. We speculated that the deletion of cytoplasmic GRK2 may accelerate the imbalance of macrophage migration-relevant pathways.

Next, we detected the macrophage function in $GRK2^{f/f}Lyz2\text{-}Cre^{+/-}$ mice. Immunofluorescence (IF) staining showed that there were fewer MHC II^+ SMs in the sublining layer of CIA $GRK2^{f/f}Lyz2\text{-}Cre^{+/-}$ mouse than in CIA $GRK2^{f/f}$ mice. In addition, the structure of the barrier-forming SMs was more complete in the CIA $GRK2^{f/f}Lyz2\text{-}Cre^{+/-}$ mice (Fig. 2b). Compared with the sham, the $CD11b^+Ly6c^+$ ratio of SMs increased in both CIA groups, and the $CD11b^+Ly6c^+$ SMs in $GRK2^{f/f}Lyz2\text{-}Cre^{+/-}$ mice was less than that in $GRK2^{f/f}$ mice (Fig. 2c). The numbers of SMs were insufficient to support more follow-up experiments, and therefore we investigated replacing SMs with BMDMs. We cultured BMDMs and SMs from 10 C57/BL6 mice and found that GRK2 expression increased in SMs compared with BMDMs (Fig. 2d) and correlated between BMDM and SM GRK2 expression (Fig. 2e), suggesting that part of the SMs originated from BMDMs. We also established an IL-1-dependent acute inflammatory arthritis model using $CCR2^{GFP/GFP}$ mice. The region of interest (ROI) values of the left synovium increased from Day 3 to Day 7 in the model group, suggesting that $CCR2^+$ MDMs were recruited into synovium (Fig. 2f).

Further, we tested the polarization and migration of BMDMs. The CD86/CD206 ratio (Fig. 2g) and cell migration (Fig. 2h) increased in both CIA groups. The CD86/CD206 macrophage ratio in $GRK2^{f/f}Lyz2\text{-}Cre^{+/-}$ mice was less than in $GRK2^{f/f}$ mice (Fig. 2g). However, the cell migration ability was higher than in $GRK2^{f/f}$ mice (Fig. 2h). These results were consistent with the LX-MultiDTM-23 results shown in Fig. S2d−S2f.

These data suggested that GRK2 deficiency attenuated the development of CIA by regulating $CCR2^+$ macrophage infiltration, while the mechanisms need to be explored.

3.3. GRK2 deficiency alters peroxisome proliferator-activated receptor γ (PPARγ) signaling in MDMs

To uncover GRK2 deficiency-induced downstream signaling, we performed RNA-seq analysis of BMDMs obtained from $GRK2^{f/f}$

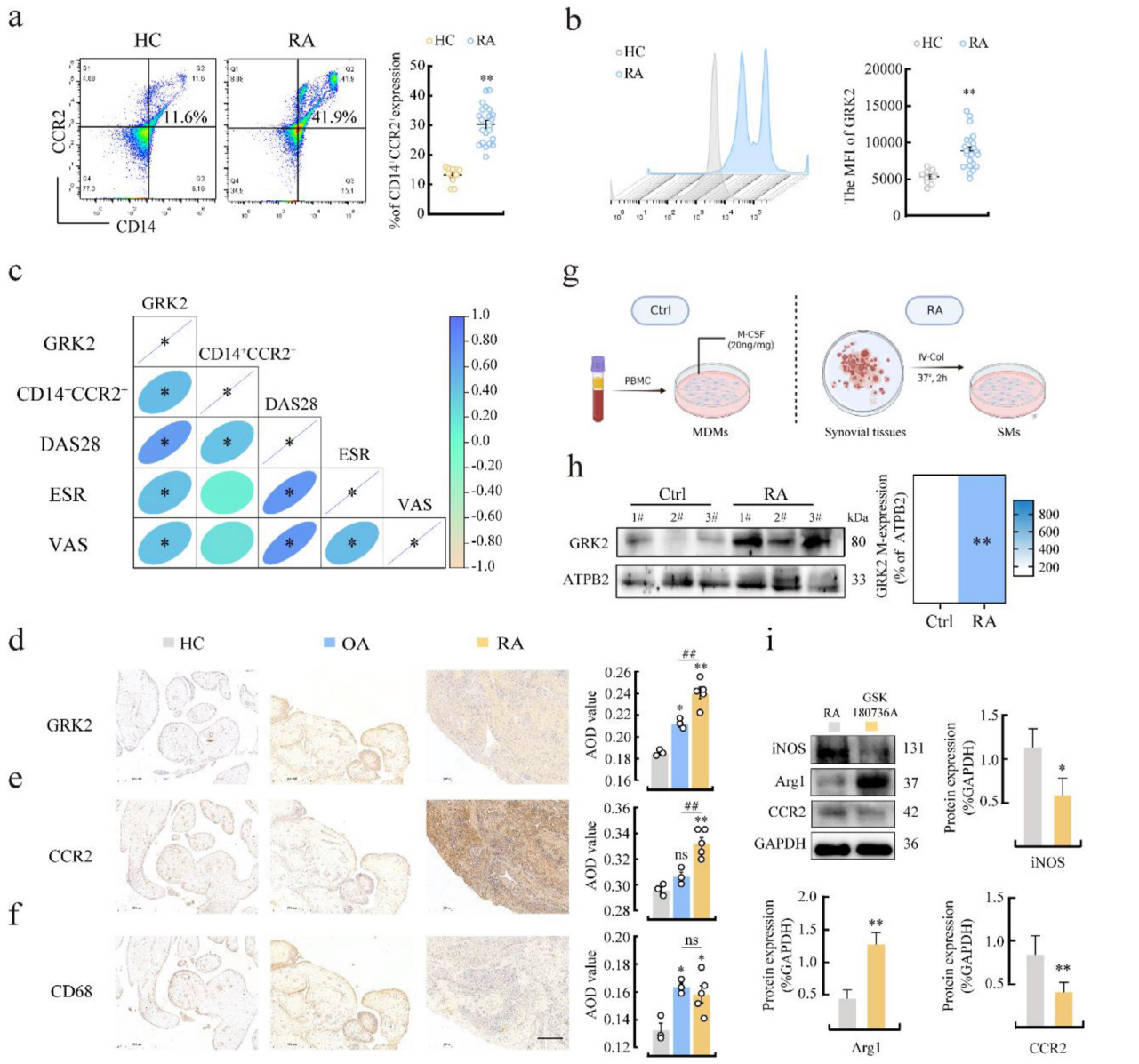

Figure 1 Increased GRK2 expression is associated with the activation of infiltrated synovial MDMs in RA. (a) Flow cytometric analysis of CD14^{+}CCR2^{+} PBMCs obtained from HCs (n = 10) and RA (n = 22). $^{**}P < 0.01$ *versus* HC. (b) Flow cytometric analysis of GRK2 MFI in PBMCs obtained from HCs (n = 10) and RA (n = 22). $^{**}P < 0.01$ *versus* HC. (c) Heat map summarizing statistically significant correlations between GRK2 and CD14^{+}CCR2^{+}, RA-related clinical manifestation (DAS28, ESR and VAS) (n = 22). $^{*}P < 0.05$. (d−f) Representative GRK2, CD68 and CCR2 immunohistochemical staining collected from HCs (n = 3), OA (n = 3) and RA (n = 5) synovium. $^{**}P < 0.01$ *versus* HC. $^{\#\#}P < 0.01$ *versus* OA. Scale bar: 500 μm. (g) Ctrl: PBMC obtained from HCs and induced by M-CSF (n = 3); RA: SM obtained from RA synovial tissue (n = 3). (h) GRK2 membraned expression of MCSF-induced PBMC. $^{**}P < 0.01$ *versus* Ctrl. (i) iNOS, Arg1 and CCR2 expression of GSK180736A-treated SM (n = 3). $^{**}P < 0.01$ *versus* RA.

and *GRK2*$^{f/f}$*Lyz2*-Cre$^{+/-}$ mice (Fig. 3a). Genes (177 total, 100 upregulated, 77 downregulated) were differentially expressed in BMDMs between two groups (Fig. 3b). Gene ontology (GO) analysis revealed that these genes were predominantly enriched in leukocyte differentiation and migration (Fig. 3c). Interestingly, the PPAR signaling pathway appeared in both the top five upregulated gene group and downregulated gene group (Fig. 3d). PPARs are nuclear hormone receptor-related transcription factors, with three different highly conserved isotypes: PPARα, PPARβ, and PPARγ[24]. First, we have assessed these three PPAR isotypes at the protein and *mRNA* level in *GRK2*$^{-/-}$ BMDMs. There was no significant difference in mRNA expression and protein expression of PPARα and PPARβ between the ctrl and *GRK2*$^{-/-}$ BMDMs (Supporting Information Fig. S3a and S3b). While PPARγ protein expression (Fig. 3f) and nuclear protein expression (Fig. 3g) decreased with unchanged mRNA expression (Fig. 3e).

PPARγ inhibited the activation and polarization of macrophages, and PPARγ agonist pioglitazone was shown to significantly improve the arthritis index[25]. Immunohistochemistry demonstrated reduced expression of PPARγ in RA synovium

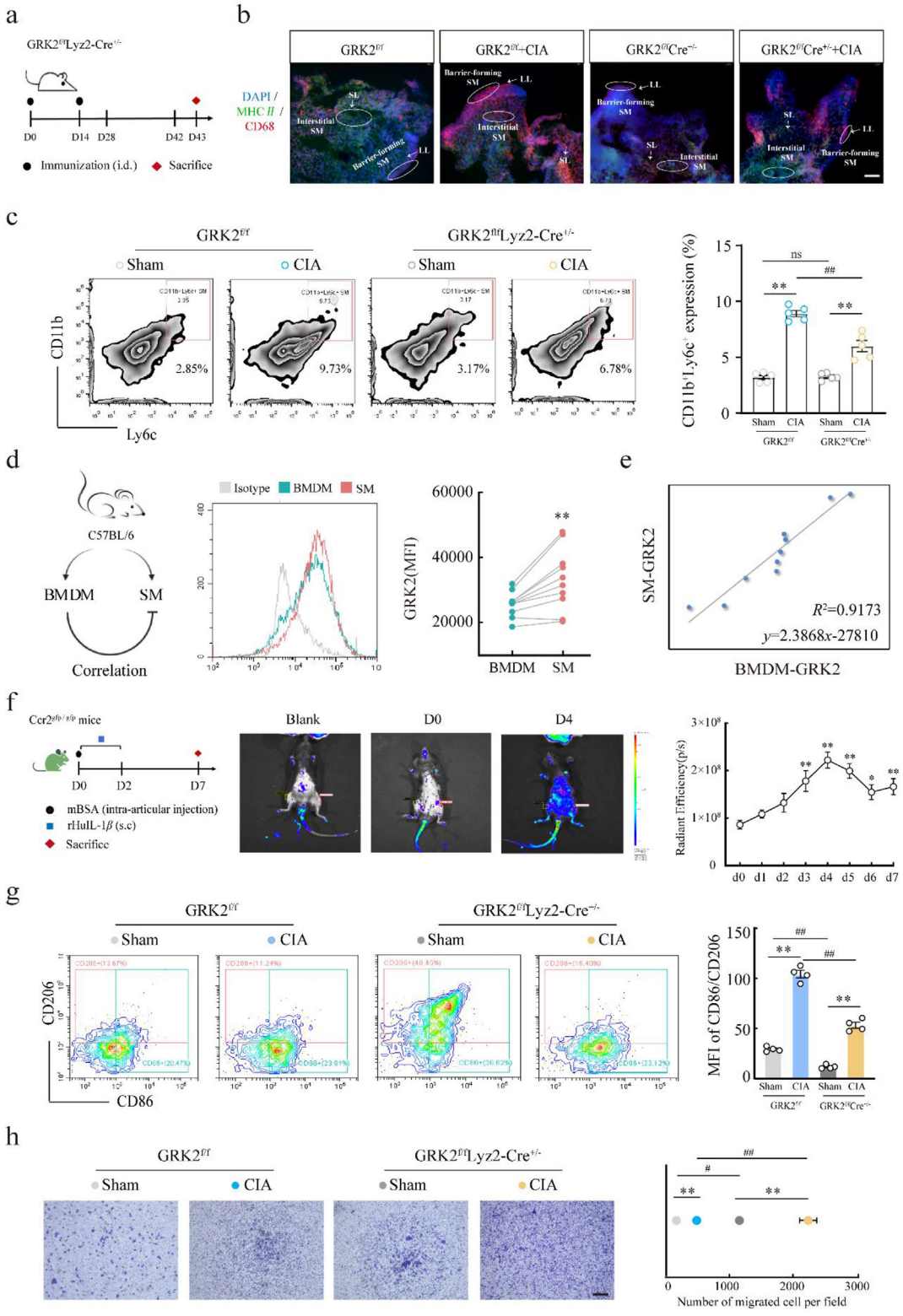

Figure 2 GRK2 deficiency attenuates the development of CIA. (a) Timeline of the experimental sequence of the CIA mouse model. (b) IF staining of MHC II in $CD68^+$ SMs ($n = 3$). LL: Lining layer. SL: Sublining layer. Scale bar: 200 μm. (c) The proportion of $CD11b^+Ly6c^+$ SM in CIA ($n = 5$), ns indicates no significant difference, $^{**}P < 0.01$ *versus* sham; $^{\#\#}P < 0.01$ *versus GRK2*$^{f/f}$. (d) GRK2 expression in BMDMs and SMs of C57/BL6 mice ($n = 10$), $^{**}P < 0.01$ *versus* BMDMs. (e) Correlations between SM-GRK2 and BMDM-GRK2 were assessed by linear regression analyses ($n = 10$). (f) Radiant efficiency of AIA synovium from Day 0 to Day 7 ($n = 5$). $^{**}P < 0.01$ *versus* Day 0. (g) The ratio of CD86/CD206 in CIA mice ($n = 4$), $^{**}P < 0.01$ *versus* sham; $^{\#\#}P < 0.01$ *versus GRK2*$^{f/f}$. (h) The BMDMs migration ability in CIA mice ($n = 3$), $^{*}P < 0.05$, $^{**}P < 0.01$ *versus* sham; $^{\#}P < 0.05$, $^{\#\#}P < 0.01$ *versus GRK2*$^{f/f}$. Scale bar: 100 μm.

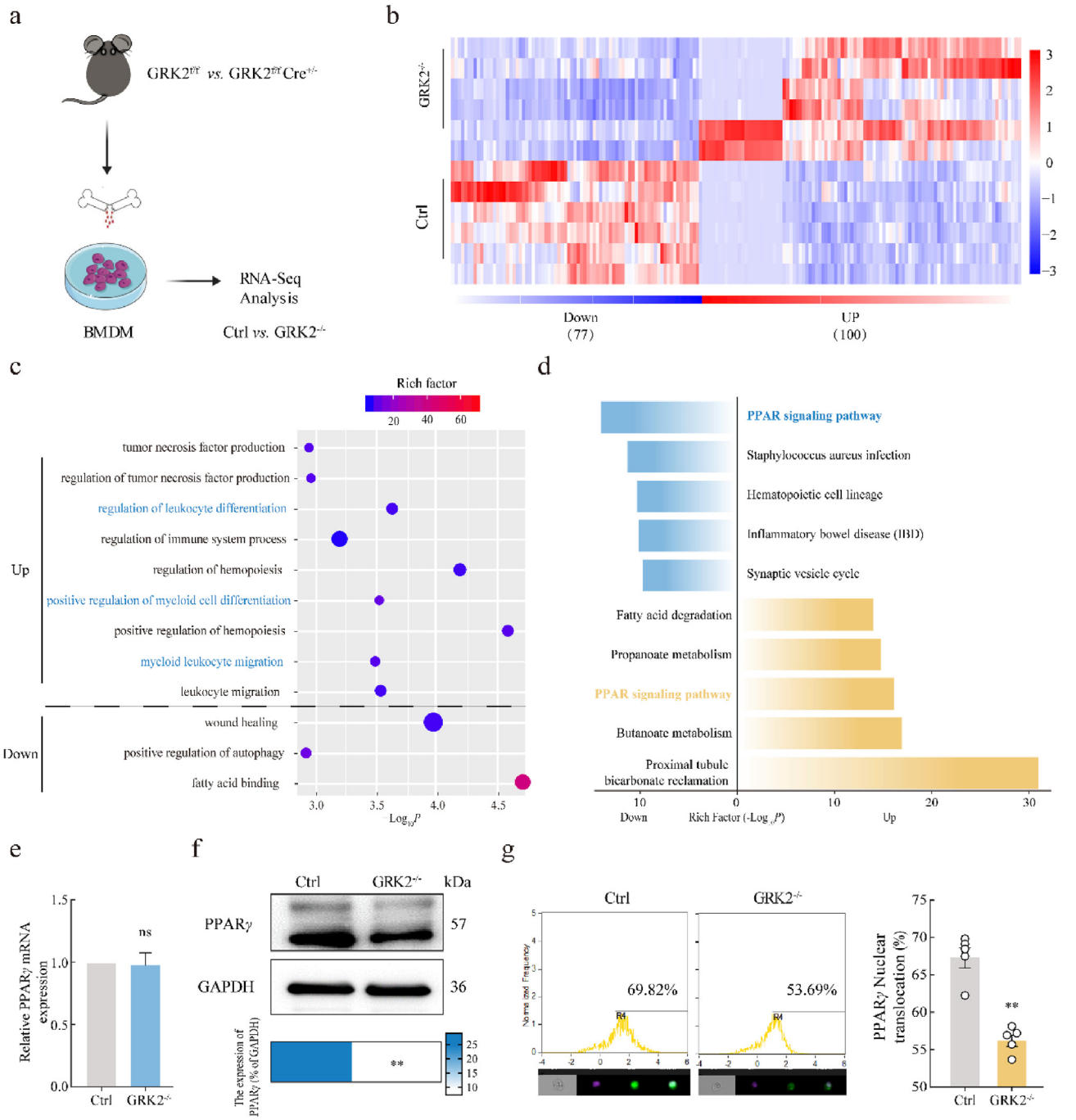

Figure 3 GRK2 deficiency alters PPARγ signaling in BMDMs. (a) RNA-seq expression analysis of BMDMs obtained from *GRK2*$^{f/f}$ ($n = 6$) and *GRK2*$^{f/f}$Cre$^{+/-}$ mice ($n = 6$). (b) Heatmap showing differential genes between BMDMs from *GRK2*$^{f/f}$ and *GRK2*$^{f/f}$Cre$^{+/-}$ mice (blue = down-regulated, red = upregulated). Fold change >2, adjusted $P < 0.05$. (c) Top-12 significantly enriched GO annotations associated with upregulated and down-regulated genes. (d) Top-10 significantly enriched KEGG pathway associated with upregulated and downregulated genes. (e) PPARγ mRNA expression of GRK2$^{-/-}$ BMDMs ($n = 3$). ns indicates no significant difference. (f) PPARγ expression of GRK2$^{-/-}$ BMDMs ($n = 6$). $^{**}P < 0.01$ *versus* Ctrl. (g) PPARγ nucleus expression of GRK2$^{-/-}$ BMDMs ($n = 5$). $^{**}P < 0.01$ *versus* Ctrl.

(Fig. S3c). However, the role of PPARγ on MDM migration in RA synovium has not been investigated. Murine BMDMs were cultured and treated with balaglitazone, a selective PPARγ agonist. We previously have demonstrated that PGE2 (10 μmol/L) can induce its receptor EP4 desensitization and GRK2 excessive membrane recruitment in Raw264.7 cells[18]. Here, we additionally provide evidence that when BMDMs were stimulated with PGE2 (10 μmol/L), a notable decrease in EP4 membrane expression was observed, accompanied by a significant increase in GRK2 membrane expression (Fig. S3d). These findings imply that the excessive desensitization of EP4 is mediated by PGE2 at a concentration of 10 μmol/L. Consequently, we employed PGE2 (10 μmol/L) to

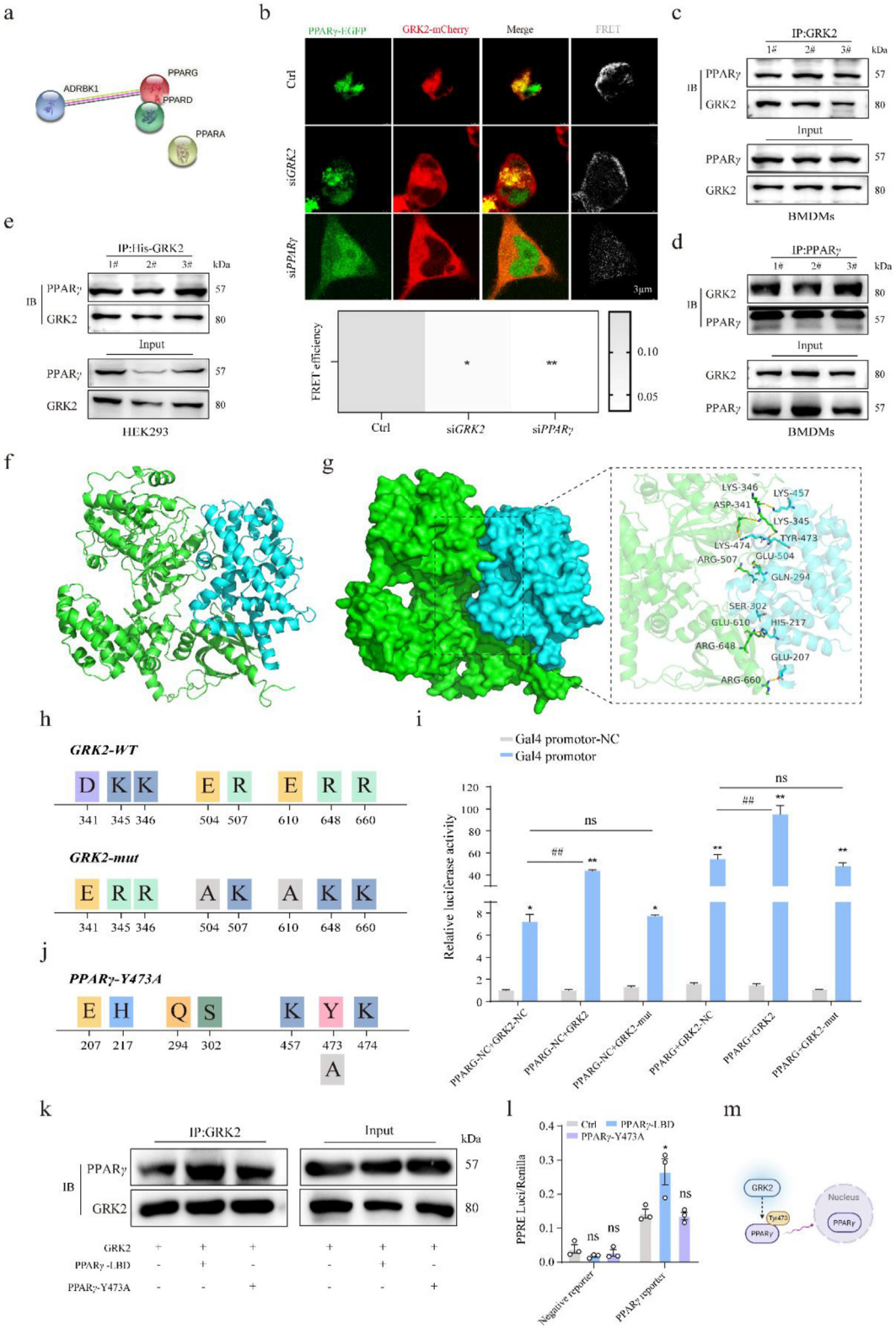

Figure 4 GRK2 activates PPARγ by targeting Tyr473. (a) PPI network of GRK2 and PPARα/β/γ. (b) FRET assay with mCherry-GRK2 and EGFP-PPARγ in HEK293 cells. Graph depicts fluorescence ratio per cell ($n = 3$). $^{*}P < 0.05$, $^{**}P < 0.01$ *versus* Ctrl. Scale bar: 3 μm. (c) The interaction between GRK2 and PPARγ in BMDMs by CO-IP, IP: GRK2 ($n = 3$). (d) The interaction between GRK2 and PPARγ in BMDMs by CO-IP, IP: PPARγ ($n = 3$). (e) The interaction of PPARγ and GRK2 in HEK293 cells by his pull-down ($n = 6$). (f) The backbone of protein was rendered in tube and colored in green. (g) GRK2 (left) and PPARγ (right) protein is rendered by the surface. The detail binding mode of GRK2 with PPARγ. Yellow dash represents hydrogen bond or salt bridge. (h) The point mutation strategy used in GRK2. (i) Luciferase reporter assay ($n = 3$), $^{*}P < 0.05$, $^{**}P < 0.01$ *versus* Gal4 promotor-NC, ns indicates no significant difference, $^{\#\#}P < 0.01$ *versus* GRK2-NC. (j) The point

simulate the transmembrane of GRK2. The migration of BMDMs and the number of CD11b$^+$CCR2$^+$ macrophages increased in the PGE2-stimulated group, and balaglitazone inhibited the proportion of CD11b$^+$CCR2$^+$ macrophages (Fig. S3e) and the migration ability of BMDMs (Fig. S3f).

There are no previous reports of GRK2 regulating the PPARγ pathway. *PPARG* (encoding PPARγ) was absent among the DEGs of the RNA-seq results. Our hypothesis posits that there may have been alterations in the protein stability or activity of PPAR.

3.4. PPARγ activation is facilitated by the targeting of PPARγ Tyr473 by GRK2

To understand why PPARγ protein expression was reduced with GRK2 deficiency, we first examined the direct interaction between GRK2 and PPARγ. Confocal laser scanning microscopy showed that GRK2 co-localized with PPARγ both in Raw264.7 cells (Fig. S4a) and BMDMs (Fig. S4b). STRING analysis (http://string-db.org/) identified potential physical and functional interactions between GRK2 and PPARα/β/γ. The results suggested that GRK2 interacted with PPARγ (Fig. 4a). A direct interaction between GRK2 and PPARγ was further confirmed by Förster resonance energy transfer (FRET) analysis in cultured cells. Coexpression of GRK2-mCherry and PPARγ-EGFP in HEK293 cells gave rise to FRET between the two proteins (Fig. 4b). To this end, we performed coimmunoprecipitation (Fig. 4c and d) in BMDMs and His pull-down assays in HEK293 cells (Fig. 4e). Above results suggested that GRK2 directly interacted with PPARγ and promoted PPARγ activity. To clarify the binding mode of GRK2 with PPARγ, we conducted a molecular docking analysis (Fig. 4f and g). Residues in contact between GRK2 and PPARγ formed a variety of interactions, such as salt bridges, hydrogen bonds, and hydrophobic interactions. The binding amino acids (aa) of PPARγ were primarily in the range of aa 290−500 (Fig. 4g), which located in the PPARγ ligand-binding domain (LBD)[26]. The binding region of GRK2 and PPARγ was mainly distributed in the LBD of PPARγ. To test whether GRK2 functioned through the PPARγ LBD, we fused the PPARγ LBD with the DNA-binding domain of the yeast transcription factor Gal4 protein to form a chimeric plasmid pBIND-PPARs-LBD[27]. HEK293 cells were transfected with the pBIND-PPARs-LBD plasmid, *GRK2* plasmid, and a Gal4 reporter. In addition, we preferentially mutated residues at GRK2 (Fig. 4h). Then we examined the ability of GRK2 to stimulate the activation of a Gal4 reporter using the dual-luciferase reporter system. Compared with the control group, there was increased luciferase activity of the Gal4 reporter in the *GRK2* plasmid transfected group, but no significant differences were observed in the group transfected with the mutated *GRK2* (Fig. 4i). Above findings indicated that GRK2 primarily interacts with PPARγ-LBD. It has been previously reported that Tyr473 plays a crucial role in regulating the transcriptional activation of PPARγ[43]. Molecular docking results indicated that the potential targets of GRK2-targeted PPARγ is Tyr473 (Fig. 4g, j), then we transfected HEK293 cells with the indicated plasmids (PPARγ-LBD and PPARγ Y473A mutant). Co-IP assays of PPARγ showed interaction with GRK2 that was enhanced by PPARγ-LBD plasmid transfection. Compared to PPARγ-LBD plasmid transfection, interaction decrased in PPARγ Y473A plasmid transfection (Fig. 4k). When using a PPARγ response element (PPRE) luciferase reporter system for testing nuclear translocation of PPARγ, the PPRE activity was increased by PPARγ-LBD plasmid transfection and without significant changes in PPARγ Y473A plasmid transfection (Fig. 4l). These experiments indicate that GRK2 predominantly interacts with PPARγ-LBD *via* targeting Tyr473, leading to the nuclear translocation of PPARγ (Fig. 4m).

We also examined the post-translational protein modification of PPARγ, and identified the level of ubiquitination increased in GRK2$^{-/-}$ Raw264.7 cells, whereas did not alter the acetylation and tyrosine phosphorylation in these cells (Fig. S4c). Consistently, inhibition of protein translation using cycloheximide (CHX) revealed a significantly reduced half-life of the PPARγ protein levels in the Raw264.7 cells with GRK2 deficient (Fig. S4d). In summary, on interacting with PPARγ, GRK2 was able to inhibit the ubiquitination and degradation of PPARγ.

3.5. GRK2-PPARγ deficiency promote the transcription of fms-related tyrosine kinase 1 (Flt-1)

PPARγ upon activation translocated to the nucleus to activate the transcription of specific genes[28]. To find the transcriptionally regulated genes of GRK2-activated PPARγ, we first performed RNA-seq analysis of BMDMs obtained from wild type and *PPARG* knockout mice (Fig. 5a). Genes (3778 total, 1934 upregulated, 1844 downregulated) were differentially expressed in BMDMs in *PPARG* knockout mice compared with *GRK2*$^{f/f}$ mice (Fig. 5b). Genes common to DEGs among *GRK2*$^{-/-}$ and *PPARG*$^{-/-}$ BMDMs and RA SMs were selected for further analysis, with 17 common DEGs identified by Venn diagram analysis (Fig. 5c). RNA-seq data of RA SMs were obtained from GSE97779 (human MDMs *vs.* RA synovial fluid macrophages) (Supporting Information Fig. S5). These 17 genes were further analyzed by KEGG pathway enrichment (Fig. 5d), and then we explored the prior literature and finally focused on the gene fms-related tyrosine kinase 1, *FLT1*. Interestingly, *FLT1* also appeared in the top 10 transcription factors enriched by up- and down-regulated DEGs in *GRK2*$^{-/-}$ BMDMs (Fig. 5e). Flt-1, also known as vascular endothelial growth factor receptor 1 (VEGFR-1), has been shown to be a novel cell surface marker for the lineage of monocytes/macrophages in humans[29]. The deletion of the tyrosine kinase domain of Flt-1 decreased the incidence and clinical symptoms of RA by modulating the proliferation of bone marrow hematopoietic cells and immunity of MDMs[30]. Here we confirmed that *FLT1* mRNA expression was significantly increased in *GRK2*$^{-/-}$ (Fig. 5f) and *PPARG*$^{-/-}$ (Fig. 5g) BMDMs. As such, how might PPARγ transcriptionally regulate Flt-1 warranted in-depth examinations (Fig. 5h)?

3.6. Flt-1 promotes MDMs migration to drive angiogenesis

We generated stable *GRK2*$^{-/-}$ Raw264.7 cell lines using the CRISPR/Cas9-mediated gene editing system[18] (Fig. 6a). Flt-1

mutation strategy used in PPARγ. (k) The interaction between GRK2 and PPARγ in HEK293 cells. HEK293 cells were co-transfected with GRK2 plasmid and PPARγ-LBD plasmid or PPARγ-Y473A plasmid ($n = 3$). (l) The activity of PPRE is measured by luciferase reporter system. HEK293T cells are co-transfected with PPARγ-LBD plasmid or PPARγ-Y473A plasmid and PPARγ reporter for 24 h ns indicates no significant difference, $^*P < 0.05$ *versus* Ctrl ($n = 3$). (m) GRK2 interacts with PPARγ *via* targeting Tyr473, leading to the nuclear translocation of PPARγ.

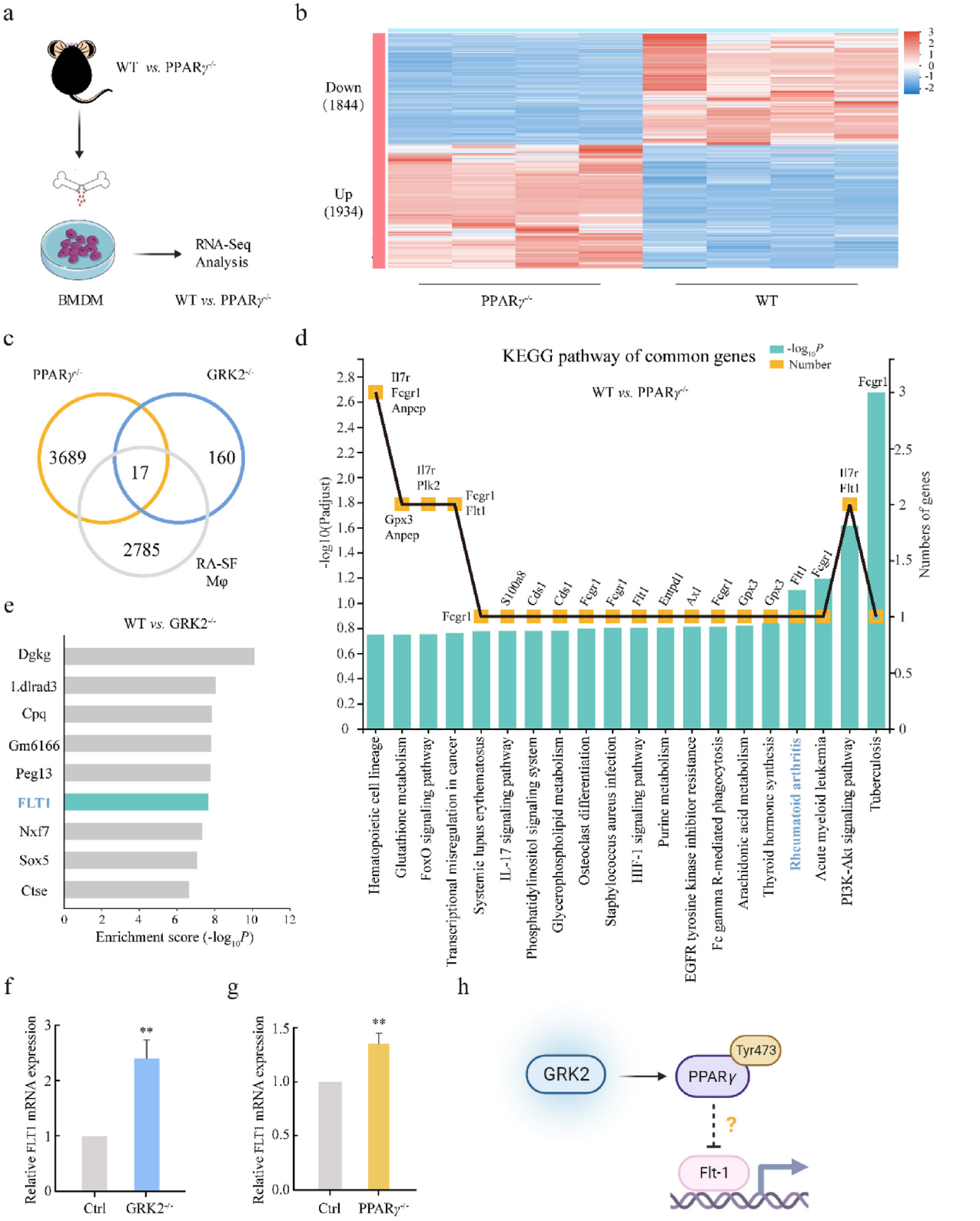

Figure 5 GRK2-PPARγ inhibited Flt-1 transcription. (a) RNA-seq expression analysis of BMDMs obtained from WT ($n = 4$) and *PPARG* knockout mice ($n = 4$). (b) Heatmap showing differential genes between BMDMs from WT and *PPARG* knockout mice (blue = down-regulated, red = upregulated). Fold change >2, adjusted $P < 0.05$. (c) *Venn* diagram indicating overlapping DEGs between GRK2$^{-/-}$, PPARγ$^{-/-}$ BMDMs and RA-SM. (d) KEGG pathway enrichment chord diagram of 17 overlapping DEGs. (e) Top 10 TFs enriched by up- and downregulated DEGs in GRK2$^{-/-}$ BMDMs. (f) Flt-1 mRNA expression in GRK2$^{-/-}$ BMDMs ($n = 3$), $^{**}P < 0.01$ *versus* Ctrl. (g) Flt-1 mRNA expression in PPARγ$^{-/-}$ BMDMs ($n = 3$), $^{**}P < 0.01$ *versus* Ctrl. (h) GRK2 activated PPARγ-Tyr473 may inhibit Flt-1 transcription.

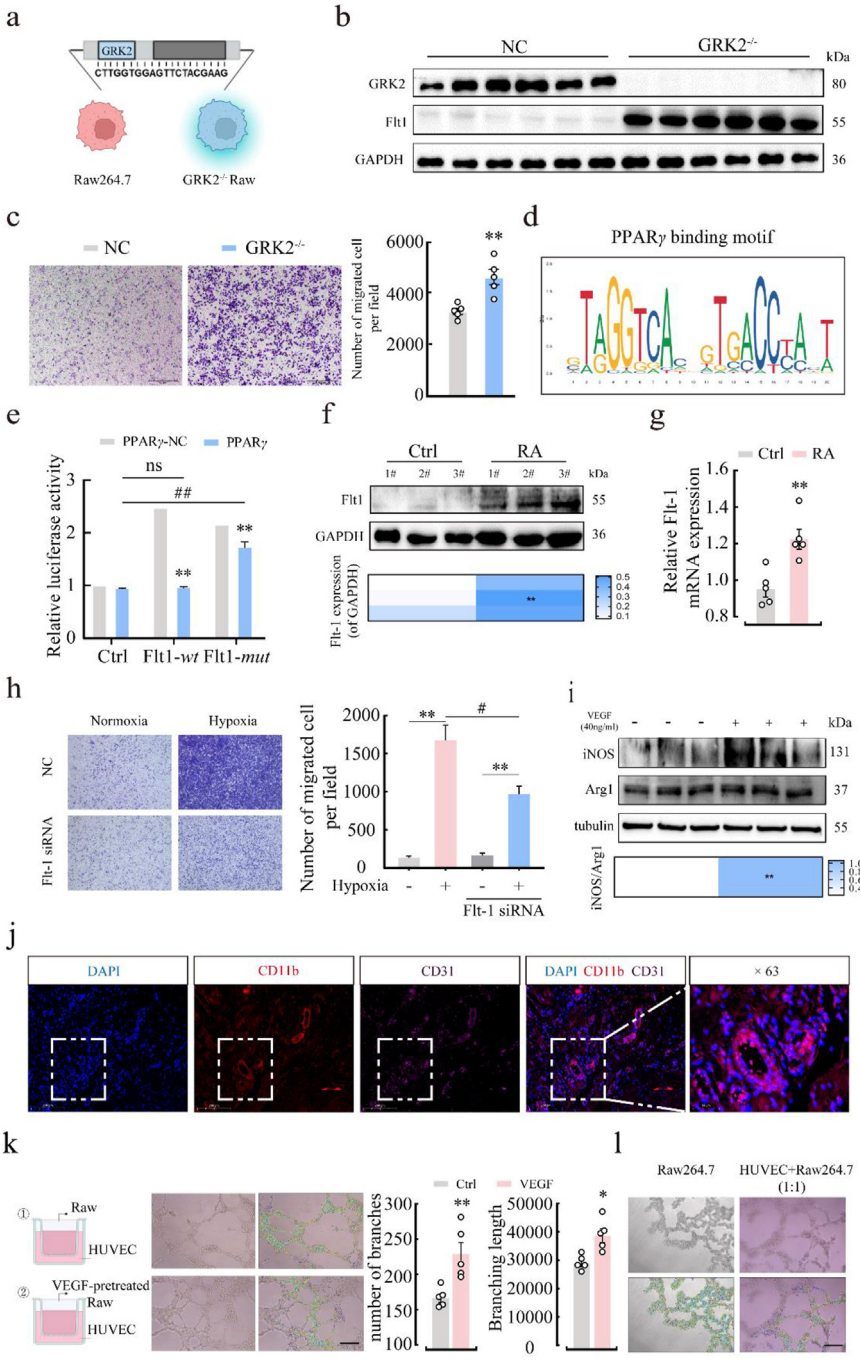

Figure 6 PPARγ inhibits the transcription of Flt-1 and results in angiogenesis. (a) The strategy for constructing GRK2$^{-/-}$ Raw264.7 cells. (b) The Flt-1 expression in GRK2$^{-/-}$ Raw264.7 cells ($n = 6$). (c) The cell migration ability of GRK2$^{-/-}$ Raw264.7 cells ($n = 5$), $^{**}P < 0.01$ *versus* NC. Scale bar: 100 μm. (d) PPARγ binding motif. (e) Luciferase reporter assay ($n = 3$), $^{**}P < 0.01$ *versus* PPARγ-NC, ns indicates no significant difference, $^{\#\#}P < 0.01$ *versus* ctrl. (f) Flt-1 expression in RA SM ($n = 3$), $^{**}P < 0.01$ *versus* Ctrl. (g) Flt-1 mRNA expression in RA SM ($n = 3$), $^{**}P < 0.01$ *versus* Ctrl. (h) The cell migration assay of Flt-1 knockdown BMDMs exposed to hypoxia ($n = 3$), $^{**}P < 0.01$ *versus* Ctrl. Scale bar: 100 μm. (i) The expression of iNOS, Arg1 and CCR2 in VEGF-stimulated BMDMs ($n = 3$). (j) IF staining for CD31 and CD11b in RA synovium ($n = 3$). Scale bar: 200 μm. (k) Tubulogenesis assays on HUVECs that were coclutred with Raw264.7 (control) or with VEGF-pretreated Raw264.7 ($n = 5$), $^{**}P < 0.01$ *versus* Ctrl. Scale bar: 100 μm. (l) Tubulogenesis assays on Raw264.7 and HUVECs mixed with Raw264.7 ($n = 5$). Scale bar: 100 μm.

expression (Fig. 6b) and cell migration (Fig. 6c) were significantly increased in these cell lines. The findings from multiplex immunohistochemistry (mIHC) analysis demonstrated a significant upregulation of GRK2 expression in CD11b^{+}Flt-1^{+} macrophages in RA compared to OA, as well as the CD11b^{+}Flt-1^{+}GRK2^{+} cell intensity (Supporting Information Fig. S6a). Furthermore, the expression levels of both GRK2 and Flt-1 were observed to be elevated in lipopolysaccharide (LPS)-induced M1 macrophages

(Fig. S6b). To further assess the role of PPARγ on Flt-1, we discovered putative PPARγ binding elements within the Flt-1 promoter region through the website hTFtarget (Fig. 6d). Next, we performed transcriptional assays to confirm the targeting relationship between PPARγ and Flt-1. The dual-luciferase reporter assay showed that co-transfection of wild-type *FLT1* with *PPARG* in HEK293 cells decreased luciferase activity as compared with either the control group or co-transfection using mutated *FLT1* (Fig. 6e). While luciferase activity also decreased in the mutated *FLT1* group, which suggested the presence of other binding sites, our results confirmed that PPARγ inhibited Flt-1 activity. We further examined Flt-1 expression in SMs, the protein expression (Fig. 6f) and mRNA expression (Fig. 6g) of Flt-1 increased in RA. We then questioned what the specific role of these Flt-1$^+$ MDMs was in RA synovium.

Flt-1 induced macrophages migration[29], and hypoxia in RA synovium may enhance this. Here we transfected murine BMDMs with *FLT1* siRNA and tested their migration under hypoxia environments. An increased cell migration ability was observed in BMDMs under hypoxia, while *FLT1* siRNA attenuated this ability (Fig. 6h). We investigated the effects of murine BMDM polarization by pretreatment with the Flt-1 agonist VEGF, the iNOS/Arg1 ratio increased in the VEGF-treated group, while it decreased compared with the control (Fig. 6i). We also explored the distribution of CD11b$^+$ SMs and CD31$^+$ endothelial cells in the RA synovium, and noticed that some of the CD11b$^+$ SMs surrounded blood vessels (Fig. 6j). Inflammatory macrophages have been shown to drive angiogenesis in multiple animal models[31]. We hypothesized that increased Flt-1$^+$ macrophages may stimulate endothelial cell behavior, with resulting effects on vascularization. HUVEC tube formation assays were performed to assess this possibility. As compared to co-cultured Raw264.7 cells, VEGF-treated Raw264.7 cells increased the ability of HUVECs to form tubes in Matrigel (Fig. 6k). In addition, a study published in 2020 reported that macrophages wrapped around and bridged adjacent vessels and formed vessel-like structures in a three-dimensional (3D) tissue-engineered human blood vessel networks *in vitro*[32]. Next, we sought to test the ability of macrophages to form vessel-like structures in Matrigel. Although Raw264.7 cells gathered and circled, it was difficult to identify vessel-like structures (Fig. 6l). Moreover, we mixed HUVEC with Raw264.7 cells (1:1) and found that macrophages surrounded the HUVECs and bridged adjacent vessels (Fig. 6l). Taken together, we confirmed that GRK2 targeted the PPARγ Tyr473, thus regulating the activation of Flt-1$^+$ macrophages. The excess GRK2 membrane recruitment in RA MDMs resulted in reduced PPARγ signaling and increased *FLT1* transcription.

3.7. CP-25 restores GRK2-PPARγ interaction to inhibit Flt-1$^+$ macrophage activation in CIA

CP-25 is a GRK2 activity inhibitor developed by our group (Fig. 7a). Previous studies demonstrated the therapeutic role of CP-25 (17.5, 35, or 70 mg/kg) in CIA mice by inhibiting Ala321 of GRK2[13,17]. In this study, we established a CIA mice model and administered the CIA mice CP-25 (35 mg/kg) for 21 days (Fig. 7b). Paw swelling, synovial inflammation, bone erosion, and the number of osteoclasts increased in CIA, CP-25 and etanercept ameliorated these changes (Fig. 7c and d). Flow cytometric analysis revealed an increase of infiltrated SMs (CD11b$^+$Ly6c$^+$) and a decrease in homeostatic macrophages (CD11b$^+$Mertk$^+$) in CIA mice (Fig. 7e). CP-25 reduced CD11b$^+$Ly6c$^+$ expression, but had no effect on CD11b$^+$Mertk$^+$ expression in SMs (Fig. 7e). The linear distribution suggested a certain level of correlation between Ly6c-SMs and Ly6c-MDMs (Fig. 7f). An increase of CD11b$^+$Ly6c$^+$BMDMs, as well as the CD86/CD206 ratio were observed in BMDMs (Supporting Information Fig. S7a and S7b). CP-25 reduced CD11b$^+$Ly6c$^+$ expression and CD86/CD206 ratio in CIA BMDMs (Fig. S7a and S7b). We then analyzed CD11b$^+$Flt-1$^+$ SMs by ankle section staining, and the proportion of CD11b$^+$Flt-1$^+$ SMs increased in the CIA mice but decreased after CP-25 treatment (Fig. 7g). We have demonstrated a correlation between BMDM and SM GRK2 expression, as shown in Fig. 2e. Next, we assessed PPARγ signal in BMDMs. Western blot analysis (Fig. 7h) showed increased membrane expression of GRK2 and decreased cytoplasmic expression of GRK2 in CIA BMDMs, which was reversed with CP-25 treatment. Similarly, decreased PPARγ and increased Flt-1 expression were observed in CIA BMDMs, which was restored with CP-25 treatment (Fig. 7h). The coimmunoprecipitation experiments identified diminished GRK2-PPARγ interactions in CIA BMDMs, which returned to basal conditions after CP-25 treatment (Fig. 7i). *In vitro*, we cultured CIA BMDMs and treated with CP-25 (1 μmol/L). Paroxetine (Paxil) (2.5 μmol/L) was selected as the positive control for its role on inhibiting GRK2 with selectivity over other GRKs[11]. Result showed that GRK2-PPARγ interaction decreased in CIA BMDMs, while restored by CP-25 and Paxil treatment (Fig. S7c). Furthermore, we also excluded the possibility that CP-25 might occupy the GRK2-PPARγ binding site. We cultured BMDMs from normal C57/BL mice and treated them with CP-25 (1 μmol/L) and Paxil (2.5 μmol/L). The interaction was not significantly different between untreated and treated (CP-25 or Paxil) BMDMs (Fig. 7j).

Finally, we used PGE2 (10 μmol/L) to stimulate the excess recruitment of GRK2 (Supporting Information Fig. S8a). We cultured PBMC-induced MDMs obtained from HCs as 3D spheroids using a PrimeSurface 96U 3D cell culture plate (Fig. S8b). The CD14$^+$CCR2$^+$ proportion (Fig. S8c), CD86/CD206 macrophage ratio (Fig. S8d), and cell migration ability (Fig. S8e) increased in PGE2-induced MDMs and decreased in the CP-25-treated group. Further, we co-cultured HUVEC cells with PBMC-induced MDMs pre-stimulated with different concentrations of CP-25 (Fig. S8f). PGE2-treated MDMs increased the ability of HUVECs to form tubes in Matrigel which decreased with CP-25 (0.1, 1, and 10 μmol/L) treatment (Fig. S8g and S8h). Consistently, the expression of CCR2 and GRK2 increased in PGE2-treated MDMs, while decreased with CP-25 (0.1, 1, and 10 μmol/L) treatment (Fig. S8i). Above results suggested that CP-25-mediated attenuation of MDMs infiltration and angiogenesis is closely associated with the inhibition of GRK2 expression.

4. Discussion

As the etiology and pathogenesis of RA remain poorly understood, effective therapies with limited adverse drug reactions are still lacking[33]. Furthermore, the complex synovial microenvironment has also made the therapeutic elimination of RA impossible for decades[34]. It is therefore important to identify common targets to restore heterogeneous cell functions for RA treatment. The

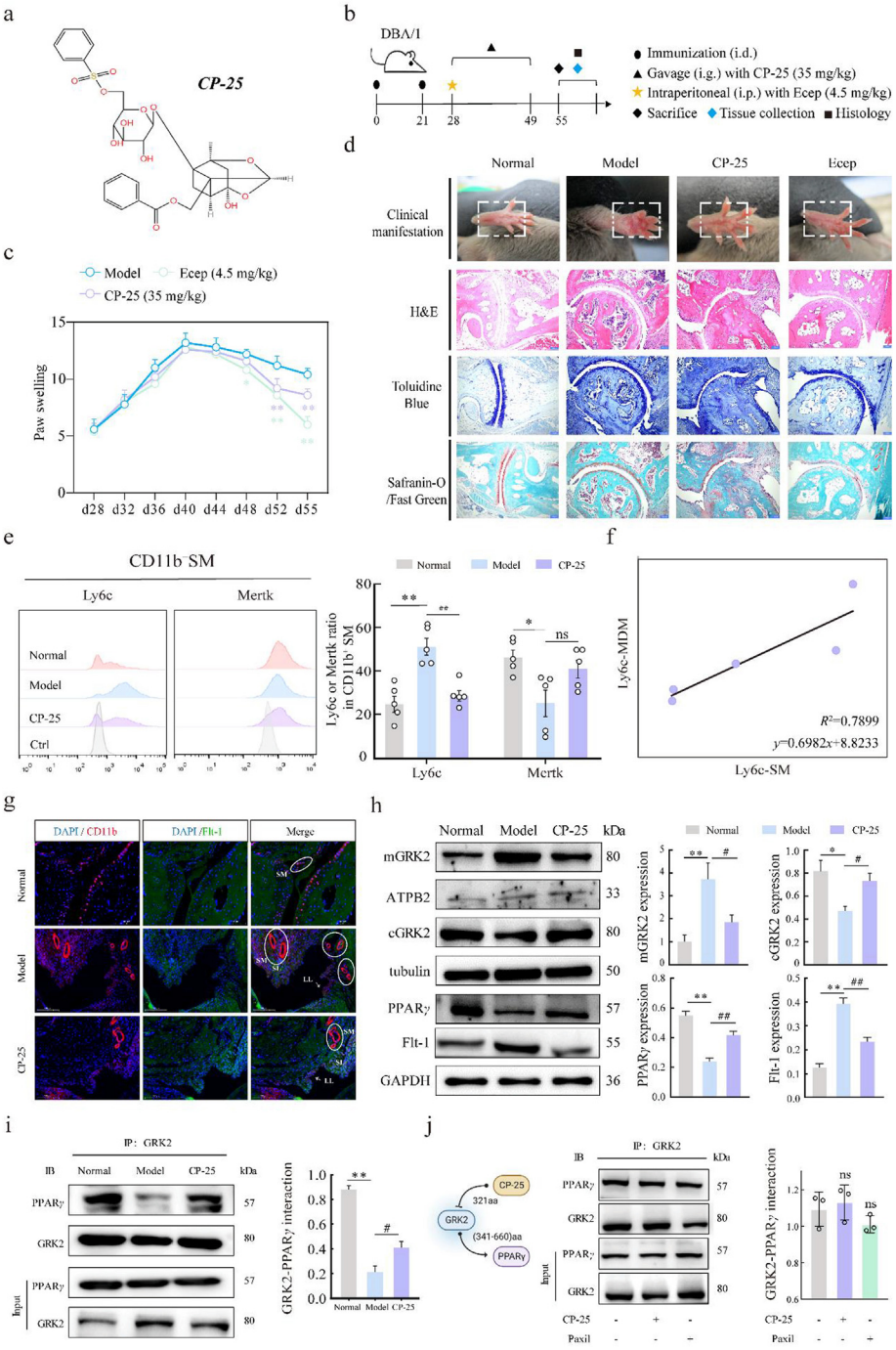

Figure 7 The role and mechanisms of GRK2 activity inhibitor on RA macrophages. (a) The structure of CP-25. (b) Timeline of the experimental sequence of the CIA mouse model ($n = 8$). (c) Paw swelling of CIA mice from Day 28 to Day 55 ($n = 8$), $^{*}P < 0.05$, $^{**}P < 0.01$ *versus* Model. (d) Representative images of ankle joint histology, H&E, toluidine blue, and safranin o−fast green staining from mice harvested at Day 55 of CIA ($n = 8$). Scale bar: 100 μm. (e) The proportion of CD11b^{+}Ly6c^{+} SM in CIA ($n = 5$), $^{*}P < 0.05$, $^{**}P < 0.01$ *versus* Normal; ns indicates no significant difference, $^{\#\#}P < 0.01$ *versus* Model. (f) Correlations between SM-Ly6c and BMDM-Ly6c were assessed by linear regression analyses ($n = 5$). (g) Immunofluorescent staining of CD11b and Flt-1 were performed on paraffin embedded ankle joint slices ($n = 5$). Scale bar: 100 μm. (h) Membrane GRK2, cytoplasm GRK2, PPARγ and Flt-1expressionin CIA BMDMs ($n = 5$), $^{*}P < 0.05$, $^{**}P < 0.01$ *versus* Normal; $^{\#\#}P < 0.01$ *versus* Model. (i) The interactions between GRK2 and PPARγ in CIA BMDMs by CO-IP ($n = 5$), $^{*}P < 0.05$, $^{**}P < 0.01$ *versus* Normal; $^{\#\#}P < 0.01$ *versus* Model. (j) The interactions between GRK2 and PPARγ in CP-25/Paxil-treated BMDMs by CO-IP ($n = 3$), ns indicates no significant difference.

dynamic plasticity of macrophages is regulated by the local microenvironment, which makes it possible to target macrophages for RA precision treatments[35,36]. We also established a strong correlation between Ly6c^{+} SMs and Ly6c^{+} BMDMs. In this study, we proved that inhibiting GRK2 activity of MDMs prevents synovial inflammation and angiogenesis.

GRK2 functional imbalance is associated with its excessive membrane recruitment, and the regulation of its activity is often more important than simply its expression level. While the role of GRK2 in RA-related immune cells both *in vitro* and *in vivo* has been reported, we analyzed the correlation between GRK2 expression and clinical indicators of RA for the first time, and the expression of GRK2 in synovium was compared among HC and OA and RA patients. GRK2 has been intensively studied, largely focused on GPCR. However, the GRK2 interactome and its modulation mechanisms in RA have been understudied. By integrating RNA-seq, we uncovered a novel GRK2-interacting protein, PPARγ. In addition, previous reports on RA macrophages have mainly focused on promoting synovial inflammation and bone destruction. Here, we discovered that GRK2-regulated Flt-1^+ macrophages stimulated endothelial cell behavior, with resulting effects on vascularization. Whether Flt-1^+ macrophages formed vessel-like structures in RA and other still unrecognized roles of these macrophages remain to be further studied.

This study still had some limitations that deserve emphasis. Cytoplasmic GRK2 decreased and GRK2 membranous recruitment increased in RA. However, *GRK2*$^{f/f}$*Lyz2*-Cre$^{+/-}$ mice cannot simulate this situation. We observed macrophage polarization toward M2 in *GRK2*$^{f/f}$*Lyz2*-Cre$^{+/-}$ mice and the migration of these macrophages was enhanced. The change of macrophage function is a multistep process regulated by numerous signals. We previously proved GRK2 membrane recruitment induced-GPCR signals imbalance increased M1 polarization, here we first demonstrated that GRK2-PPARγ signals inhibited CCR2$^+$ MDMs M1 polarization and migration.

In summary, targeting GRK2 activity is a viable strategy to inhibit CCR2$^+$ MDMs infiltration, affording a distinct way to control joint inflammation and angiogenesis of RA.

Acknowledgments

We thank LetPub (www.letpub.com) for its linguistic assistance during the preparation of this manuscript. We thank all the patients who participated in providing us with synovial tissues and blood samples. Graphical abstract was created with BioRender.com (publication and licensing rights number JZ25ROGTF8). This study was supported by the National Natural Science Foundation of China (No. 82003763, No. 81973332, No. 82173824, No. 82204405, No. 82204402), Research Fund of Anhui Institute of translational medicine (2022zhyx-B04, China), The 2022 Basic and Clinical Collaborative Research of Anhui Medical University (2022sfy015, China), and Natural Science Foundation of Anhui Provincial (2108085QH383, China).

Author contributions

Wei Wei and Xuezhi Yang conceived and designed the experiments. Xuezhi Yang, Yingjie Zhao, Qi Wei, Wankang Zhang, Luping Wang, Xuemin Zhu, and Xiaoyi Liu performed the experiments. Xuezhi Yang and Yingjie Zhao analyzed the data. Wei Wei and Xuezhi Yang contributed reagents/materials/analysis tools. Xuezhi Yang and Wei Wei contributed to writing the manuscript.

Conflicts of interest

The authors have no conflicts of interest to declare.

Appendix A. Supporting information

Supporting data to this article can be found online at https://doi.org/10.1016/j.apsb.2023.09.013.

References

1. Safiri S, Kolahi AA, Hoy D, Smith E, Bettampadi D, Mansournia MA, et al. Regional and national burden of rheumatoid arthritis 1990–2017: a systematic analysis of the Global Burden of Disease study 2017. *Ann Rheum Dis* 2019;**78**:1463–71.
2. Udalova IA, Mantovani A, Feldmann M. Macrophage heterogeneity in the context of rheumatoid arthritis. *Nat Rev Rheumatol* 2016;**12**:472–85.
3. Tu J, Hong W, Guo Y, Zhang P, Fang Y, Wang X, et al. Ontogeny of synovial macrophages and the roles of synovial macrophages from different origins in arthritis. *Front Immunol* 2019;**10**:1146.
4. Culemann S, Grüneboom A, Nicolás-Ávila JÁ, Weidner D, Lämmle KF, Rothe T, et al. Locally renewing resident synovial macrophages provide a protective barrier for the joint. *Nature* 2019;**572**:670–5.
5. Alivernini S, MacDonald L, Elmesmari A, Finlay S, Tolusso B, Gigante MR, et al. Distinct synovial tissue macrophage subsets regulate inflammation and remission in rheumatoid arthritis. *Nat Med* 2020;**26**:1295–306.
6. Misharin AV, Cuda CM, Saber R, Turner JD, Gierut AK, Haines 3rd GK, et al. Nonclassical Ly6C (−) monocytes drive the development of inflammatory arthritis in mice. *Cell Rep* 2014;**9**:591–604.
7. Weiss M, Byrne AJ, Blazek K, Saliba DG, Pease JE, Perocheau D, et al. IRF5 controls both acute and chronic inflammation. *Proc Natl Acad Sci U S A* 2015;**112**:11001–6.
8. Yang X, Chang Y, Wei W. Emerging role of targeting macrophages in rheumatoid arthritis: focus on polarization, metabolism and apoptosis. *Cell Prolif* 2020;**53**:e12854.
9. Tu J, Chen W, Fang Y, Han D, Chen Y, Jiang H, et al. PU.1 promotes development of rheumatoid arthritis *via* repressing FLT3 in macrophages and fibroblast-like synoviocytes. *Ann Rheum Dis* 2023;**82**:198–211.
10. Schumacher SM, Gao E, Zhu W, Chen X, Chuprun JK, Feldman AM, et al. Paroxetine-mediated GRK2 inhibition reverses cardiac dysfunction and remodeling after myocardial infarction. *Sci Transl Med* 2015;**7**:277ra31.
11. Carlson EL, Karuppagounder V, Pinamont WJ, Yoshioka NK, Ahmad A, Schott EM, et al. Paroxetine-mediated GRK2 inhibition is a disease-modifying treatment for osteoarthritis. *Sci Transl Med* 2021;**13**:eaau8491.
12. Evron T, Daigle TL, Caron MG. GRK2: multiple roles beyond G protein-coupled receptor desensitization. *Trends Pharmacol Sci* 2012;**33**:154–64.
13. Han C, Li Y, Zhang Y, Wang Y, Cui D, Luo T, et al. Targeted inhibition of GRK2 kinase domain by CP-25 to reverse fibroblast-like synoviocytes dysfunction and improve collagen-induced arthritis in rats. *Acta Pharm Sin B* 2021;**11**:1835–52.
14. Cheloha RW, Fischer FA, Woodham AW, Daley E, Suminski N, Gardella TJ, et al. Improved GPCR ligands from nanobody tethering. *Nat Commun* 2020;**11**:2087.
15. Thal DM, Homan KT, Chen J, Wu EK, Hinkle PM, Huang ZM, et al. Paroxetine is a direct inhibitor of g protein-coupled receptor kinase 2 and increases myocardial contractility. *ACS Chem Biol* 2012;**7**:1830–9.
16. Norel X, Sugimoto Y, Ozen G, Abdelazeem H, Amgoud Y, Bouhadoun A, et al. International union of basic and clinical pharmacology. CIX. Differences and similarities between human and rodent prostaglandin E2 receptors (EP1–4) and prostacyclin peceptor (IP): specific roles in pathophysiologic conditions. *Pharmacol Rev* 2020;**72**:910–68.
17. Yang XZ, Wei W. CP-25, a compound derived from paeoniflorin: research advance on its pharmacological actions and mechanisms in

the treatment of inflammation and immune diseases. *Acta Pharmacol Sin* 2020;**41**:1387−94.
18. Yang X, Li S, Zhao Y, Li S, Zhao T, Tai Y, et al. GRK2 mediated abnormal transduction of PGE2-EP4-cAMP-CREB signaling induces the imbalance of macrophages polarization in collagen-induced arthritis mice. *Cells* 2019;**8**:1596.
19. Bosakova M, Abraham SP, Nita A, Hruba E, Buchtova M, Taylor SP, et al. Mutations in GRK2 cause Jeune syndrome by impairing Hedgehog and canonical Wnt signaling. *EMBO Mol Med* 2020;**12**: e11739.
20. Li RC, Haribabu B, Mathis SP, Kim J, Gozal D. Leukotriene B4 receptor-1 mediates intermittent hypoxia-induced atherogenesis. *Am J Respir Crit Care Med* 2011;**184**:124−31.
21. Geissmann F, Manz MG, Jung S, Sieweke MH, Merad M, Ley K. Development of monocytes, macrophages, and dendritic cells. *Science* 2010;**327**:656−61.
22. Choi S, You S, Kim D, Choi SY, Kwon HM, Kim HS, et al. Transcription factor NFAT5 promotes macrophage survival in rheumatoid arthritis. *J Clin Invest* 2017;**127**:954−69.
23. Wu J, Feng Z, Chen L, Li Y, Bian H, Geng J, et al. TNF antagonist sensitizes synovial fibroblasts to ferroptotic cell death in collagen-induced arthritis mouse models. *Nat Commun* 2022;**13**:676.
24. van der Meer DL, Degenhardt T, Väisänen S, de Groot PJ, Heinäniemi M, de Vries SC, et al. Profiling of promoter occupancy by PPARalpha in human hepatoma cells *via* ChIP-chip analysis. *Nucleic Acids Res* 2010;**38**:2839−50.
25. Liu Y, Wang J, Luo S, Zhan Y, Lu Q. The roles of PPARγ and its agonists in autoimmune diseases: a comprehensive review. *J Autoimmun* 2020;**113**:102510.
26. Luan P, Jian W, Xu X, Kou W, Yu Q, Hu H, et al. NLRC5 inhibits neointima formation following vascular injury and directly interacts with PPARγ. *Nat Commun* 2019;**10**:2882.
27. Wei W, Wang X, Yang M, Smith LC, Dechow PC, Sonoda J, et al. PGC1beta mediates PPARgamma activation of osteoclastogenesis and rosiglitazone-induced bone loss. *Cell Metabol* 2010;**11**:503−16.
28. Mangelsdorf DJ, Thummel C, Beato M, Herrlich P, Schütz G, Umesono K, et al. The nuclear receptor superfamily: the second decade. *Cell* 1995;**83**:835−9.
29. Sawano A, Iwai S, Sakurai Y, Ito M, Shitara K, Nakahata T, et al. Flt-1, vascular endothelial growth factor receptor 1, is a novel cell surface marker for the lineage of monocyte-macrophages in humans. *Blood* 2001;**97**:785−91.
30. Murakami M, Iwai S, Hiratsuka S, Yamauchi M, Nakamura K, Iwakura Y, et al. Signaling of vascular endothelial growth factor receptor-1 tyrosine kinase promotes rheumatoid arthritis through activation of monocytes/macrophages. *Blood* 2006;**108**:1849−56.
31. Willenborg S, Lucas T, van Loo G, Knipper JA, Krieg T, Haase I, et al. CCR2 recruits an inflammatory macrophage subpopulation critical for angiogenesis in tissue repair. *Blood* 2012;**120**:613−25.
32. Graney PL, Ben-Shaul S, Landau S, Bajpai A, Singh B, Eager J, et al. Macrophages of diverse phenotypes drive vascularization of engineered tissues. *Sci Adv* 2020;**6**:eaay6391.
33. Lauper K, Iudici M, Mongin D, Bergstra SA, Choquette D, Codreanu C, et al. Effectiveness of TNF-inhibitors, abatacept, IL6-inhibitors and JAK-inhibitors in 31 846 patients with rheumatoid arthritis in 19 registers from the 'JAK-pot' collaboration. *Ann Rheum Dis* 2022;**81**:1358−66.
34. Penkava F, Velasco-Herrera MDC, Young MD, Yager N, Nwosu LN, Pratt AG, et al. Single-cell sequencing reveals clonal expansions of pro-inflammatory synovial CD8 T cells expressing tissue-homing receptors in psoriatic arthritis. *Nat Commun* 2020;**11**:4767.
35. Yin H, Zhang X, Yang P, Zhang X, Peng Y, Li D, et al. RNA m6A methylation orchestrates cancer growth and metastasis *via* macrophage reprogramming. *Nat Commun* 2021;**12**:1394.
36. Kuo D, Ding J, Cohn IS, Zhang F, Wei K, Rao DA, et al. HBEGF+ macrophages in rheumatoid arthritis induce fibroblast invasiveness. *Sci Transl Med* 2019;**11**:eaau8587.
37. Tsang JS, Schwartzberg PL, Kotliarov Y, Biancotto A, Xie Z, Germain RN, et al. Global analyses of human immune variation reveal baseline predictors of postvaccination responses. *Cell* 2014;**157**: 499−513.
38. Inglis JJ, Simelyte E, McCann FE, Criado G, Williams RO. Protocol for the induction of arthritis in C57BL/6 mice. *Nat Protoc* 2008;**3**: 612−8.
39. Allport JR, Muller WA, Luscinskas FW. Monocytes induce reversible focal changes in vascular endothelial cadherin complex during transendothelial migration under flow. *J Cell Biol* 2000;**148**: 203−16.
40. Lawlor KE, Campbell IK, O'Donnell K, Wu L, Wicks IP. Molecular and cellular mediators of interleukin-1-dependent acute inflammatory arthritis. *Arthritis Rheum* 2001;**44**:442−50.
41. Liu F, Ma F, Wang Y, Hao L, Zeng H, Jia C, et al. PKM2 methylation by CARM1 activates aerobic glycolysis to promote tumorigenesis. *Nat Cell Biol* 2017;**19**:1358−70.
42. Xiao X, Xu M, Yu H, Wang L, Li X, Rak J, et al. Mesenchymal stem cell-derived small extracellular vesicles mitigate oxidative stress-induced senescence in endothelial cells *via* regulation of miR-146a/Src. *Signal Transduct Targeted Ther* 2022;**7**:234.
43. Obermoser V, Urban ME, Murgueitio MS, Wolber G, Kintscher U, Gust R. New telmisartan-derived PPARγ agonists: impact of the 3D-binding mode on the pharmacological profile. *Eur J Med Chem* 2016; **124**:138−52.